Indian Journal of Biochemistry & Biophysics
Vol. 61, October 2024, pp. 604-619
DOI: 10.56042/ijbb.v61i10.9277

Binding interaction of Spilanthol and UDA with Malarial targets: Network pharmacology, ADME, Molecular docking, and Molecular dynamics simulation studies

Venkatramanan Varadharajan[1], Madhan Nagaraj[1], Priyanka Thangapandi[1], Govindarasu Murugavel[2] & Radhika Rajendran[1]*

[1]Department of Biotechnology, PSG College of Technology, Peelamedu, Coimbatore-641 004, Tamil Nadu, India

[2]Department of Chemistry, Thiru. Vi. Ka. Govt. Arts College, Thiruvarur-610 003, Tamil Nadu, India

Received 13 March 2024; *revised 02 July 2024*

Worldwide, the escalating global malaria crisis driven by multidrug-resistant *Plasmodium falciparum* strains necessitates the urgent need for the development of anti-malarial drug. This study employs advanced computational methodologies to assess the anti-malarial properties of (2*E*,6*Z*,8*E*)-*N*-isobutyl-2,6,8-decatrienamide (Spilanthol) and (2*E*,4*Z*)-*N*-isobutyl-2,4-undecadiene-8,10-diynamide (UDA). Previous *in vitro* studies established their anti-malarial activity; however, this research integrates network pharmacology, molecular docking, ADME analysis, and molecular dynamics simulations to unravel their potential. Utilizing Swiss Target Prediction and Super-PRED databases, potential targets for Spilanthol and UDA were predicted, intersecting with malaria-related targets from Gene Cards and OMIM databases. Protein-protein interaction networks, visualized through STRING and Cytoscape 3.10.1, highlight common targets. Molecular docking reveals Spilanthol's robust binding affinity (-27.196 kJ•mol-1) to Prostaglandin G/H synthase 2 (PTGS2), indicating its promising anti-malarial candidacy. In drug development, ADMET properties play a pivotal role; therefore, SwissADME and AdmetSAR online servers were employed for *In silico* ADME and toxicity prediction. Molecular dynamics simulations further assessed the stability and conformational dynamics of the compounds. This comprehensive in-silico investigation enhances our understanding of Spilanthol and UDA's anti-malarial potential, providing valuable insights for potential clinical trials. These findings contribute to the ongoing efforts to combat malaria, emphasizing the importance of computational approaches in drug discovery and development.

Keywords: (2*E*,4*Z*)-*N*-isobutyl-2,4-undecadiene-8,10-diynamide, (2*E*,6*Z*,8*E*)-*N*-isobutyl-2,6,8-decatrienamide, Anti-malarial activity, Malaria-related targets, Prostaglandin G/H synthase 2

Malaria colloquially referred to as one of the life threatening diseases which stands as a formidable global health challenge[1]. Globally, it is transmitted by female Anopheles mosquitoes carrying the *Plasmodium* parasite, despite ongoing efforts for control and eradication[1]. In 2020, the World Health Organization recorded 241 million malaria cases, resulting in 627,000 fatalities [2]. In general, there are five different *Plasmodium* species such as *Plasmodium falciparum*, *Plasmodium malariae*, *Plasmodium vivax*, *Plasmodium ovale*, and *Plasmodium knowlesi* are majorly responsible for causing the disease, "Malaria" in human beings[1]. Public health data from Africa estimates a significant surge ranging from 2 to 11 times in malaria-related mortality among children as they show resistance to treatments for malaria[3]. To treat malarial disease, current therapeutic recommendations involve combining artemisinin derivatives with other anti-malarials and antibiotics[4]. On the other hand, the malarial parasites have developed resistance against the first line drugs such as quinolines, naphthoquinones, antifolates, 8-aminoquinolines, and endoperoxides. Furthermore, there's growing resistance to the once-effective Artemisinin Combination Therapy (ACT) in certain regions[5,6]. In the same way, in Africa, where *P. falciparum* shows enduring resistance to Chloroquine, a longstanding antimalarial agent[3]. The drug-resistant strains of malarial parasites could be a result of a mutation in the active sites of the drug targets. Additionally, a significant challenge in malaria treatment arises from the diminished efficacy and escalating resistance of the parasite to antimalarial drugs. Therefore, there is an urgent need and on-going demand to develop novel and new potent anti-malarials.

The anti-malarial drugs which are developed have larger impact of clinical importance. The available anti-malarial drugs are derived purely from medicinal plants, including chloroquine and artemisinin[7]. These naturally derived products from the potential source of medicinal plants are referred to as secondary metabolites. Recently the exploration of the biological activity of

*Correspondence:
E-mail: rrd.bio@psgtech.ac.in; vinoth.radhika07@gmail.com

N-alkylamides has been increased in view of developing potential drugs[8]. These are plant-derived amides with a poly-unsaturated aliphatic fatty acid and an amine[8]. These *N*-alkylamides are known to pass various physiological barriers such as oral, skin, blood-brain barrier, and gut mucosa[8]. Passing these barriers during the absorption phase is the primary need for novel drugs to be authorized as biologic compound. As per the World Health Organization (WHO), approximately 80% of nations categorized as low and middle-income rely on medicinal plants as their primary source for healthcare[9]. These botanical resources readily available and associated with fewer side effects compared to conventional pharmaceuticals[10]. To attest, these *N*-alkylamides of *Spilanthes* species have been shown to possess a wider range of biological properties such as larvicidal, insecticidal, acaricidal and ant-helmintic properties[11,12]. Moreover, of various *N*-alkylamides, Spilanthol and UDA are two different compounds have been isolated from *in vitro* cultures of *Spilanthes paniculata* and evaluated for both schizonticidal and parasiticidal activity[8].

This study aimed at identifying new potential anti-malarial agents by virtual screening of two different *N*-alkylamides against prostaglandin G/H synthase 2 (PTGS2) using molecular docking analysis. The robust binding interactions were also characterized and suggest a potential mechanism by which *N*-alkylamides may exert its antimalarial effects. Hence, it can emerge as viable alternatives in the exploration for new therapeutic agents. Moreover, extending beyond in-vitro exploration, a comprehensive in-silico research investigation employing molecular dynamics (MD) simulations presents an opportunity to gain profound insights into the antimalarial potential of Spilanthol and UDA. This approach delves into the intricate binding mechanisms of PTGS2-ligand complexes, offering a nuanced understanding of their interactions at a molecular level.

Materials and Methods

Acquisition of the *N*-alkylamides corresponding targets

The two biologically active *N*-alkylamides such as (2*E*,6*Z*,8*E*)-*N*-isobutyl-2,6,8-decatrienamide (Spilanthol) and (2*E*,4*Z*)-*N*-isobutyl-2,4-undecadiene-8,10-diynamide (UDA) corresponding targets were obtained from the SwissTargetPrediction[13] and Super PRED 3.0[14] databases. Using associated targets of *N*-alkylamides on their SMILES formulas, these SMILES are retrieved from PubChem database.

Predicting targets of malaria

The GeneCards[15] and OMIM (http://OMIM.org)[16] databases has been used in order to retrieve potential malarial targets in *Homo sapiens*. Further, the targets from GeneCards that had a relevance score of >45 were selected as potential targets. Regarding the OMIM databases, all of the datasets are involved. Furthermore, the online tool Venny 2.1.0 was used to construct a Venn diagram between the *N*-alkyamides and malarial target genes for common target genes.

Network construction

Protein-protein interaction (PPI) network

The construction of protein-protein interactions was facilitated using StringDB[17], for the overlapping target genes which were retrieved from the venny 2.1.0 online tool. This PPI network reveals the influence of protein interaction relationship of Spilanthol and UDA genes with corresponding malarial genes in *Homo sapiens*. Later, the TSV file (both Excel and cytoscape) and node degree data were exported from StringDB[17]. Molecular interaction networks were also visualized using Cytoscape_v3.10.1[45] which also integrates gene expression. Then, the TSV file was imported into Cytoscape for analyzing topological properties. Finally, the core targets were retrieved by the degree of nodes in the network using the "CytoHubba" plug-in in Cytoscape.

"Gene Ontology" (GO) Functional Enrichment and "Kyoto Encyclopedia of Genes and Genomes" (KEGG) Pathway Enrichment Analysis

To study the biological process (BP), cellular component (CC), molecular function (MF) and KEGG pathway enrichment analysis, the common targets were imported to the GO pathway enrichment analysis using online tool SRPLOT[18]. The GO terms and KEGG terms with P value < 0.05 were considered as potential entries[19]. Using top 10 signal pathways, a histogram and bubble diagram were constructed which shows significant "target-pathway" network.

ADMET analysis

The SwissADME[20] online server was used to determine the drug-like properties. The two active *N*-alkylamides were imported into the SwissADME server with their respective canonical smiles downloaded from PubChem. Further, the toxicity of two active compounds were predicted by using free online tool ProTox-II[21] which reveals the predicted

LD_{50}, reverse mutation assay (Ames test) and also its cytotoxicity.

Molecular docking

All molecular docking simulations were performed using the Python library (pyRx)[22]. Virtual screening experiments were performed using AutoDock tools[22] and Open Babel[23] to generate input files for docking simulation and ligand preparation, such as energy minimization and creation of grid maps that define interaction energy between protein and ligand. In addition, the 3D structures of the core targets, identified as the top 10 based on their significance, were acquired from the RCSB Protein Data Bank (PDB; http://www.rcsb.org/pdb/)[24] in PDB format. Subsequently, the removal of water molecules and heteroatoms from the PDB structures was executed using Swiss-PDB Viewer software[25]. Subsequently, the 3D structures of Spilanthol and UDA were procured from the PubChem database in SDF format. These structures were further transformed into PDB format through the utilization of the open-source online tool known as OpenBabel. Later, macromolecules (targets) were loaded initially with energy-minimized ligand which was converted to PDBQT files after selecting the AutoDock ligands. Further, molecular docking simulation was performed under AutoDock Vina[26] wizard of PyRx. Before docking, the gird box was centred and constructed in a manner where it covers all the binding sites. The docking process involving core compounds and targets exhibited stronger binding forces with lower docking energies, and the resulting output files containing atomic coordinates were extracted for subsequent simulation.

Molecular dynamics simulations

Molecular dynamics simulations (MD) were executed to assess the stability of the protein -ligand interactions. In order to execute MD simulations Desmond v2022.1.1 was utilized. Based on the molecular docking outcomes, the most promising protein-ligand complexes for each N-alkylamide were chosen for subsequent molecular dynamics (MD) simulations. The docked complexes were immersed in the TIP3P water model[27]. To attain a neutral charge, counter ions were introduced into the docked complex systems, ensuring the maintenance of physiological salt concentration at 0.15 M. Further, Periodic boundary conditions were applied in the simulation system, and electrostatics was computed utilizing the particle mesh Ewald (PME) approach[28]. In addition, the Lennard-Jones interactions were obtained by applying a cut off distance of 10Å. Subsequently, the docked complex underwent simulation in Maestro v13.1.137, with energy minimization performed using OPLS-2005 force field parameters, followed by a relaxation step[29]. The simulation of the complex was conducted in the Berendsen NVT ensemble, maintaining a temperature of 10 K to restrict the movements of heavy atoms within the solute. In the course of MD simulations, a temperature of 300 K and pressure scale of 1 atm were maintained through the implementation of the Nose-Hoover thermostat and Martyna-Tobias-Klein barostat approach. Trajectories were recorded at intervals of 4.8 ps during the simulation, and the NPT ensemble was initiated for a production run lasting 100 ns[30]. Post-simulation, essential parameters such as root mean square fluctuations (RMSF), root mean square deviation (RMSD), and intermolecular interactions were extracted using the 'simulation interaction diagram' module of Desmond.

Radius of Gyration

The radius of gyration (R_g) is an index for monitoring the structural changes that occur during MD simulation. It also indicates the compactness of the protein complex. The lower the Rg (radius of gyration) value, the higher the rigidness of the protein during simulation[31]. The radius of gyration can be stated as,

$$R_g = \sqrt{\frac{1}{N}\sum_{i=1}^{N} r(i) - r_{centre}\mathrm{v}^2}$$

Where r(i) refers to coordinates of atom i,

N refers to the number of protein atoms,

r_{centre} refers to the center of mass[32]. The structural variation that occurs during MD simulation is quantified using the above formula.

Monitoring of Hydrogen bond interactions

A hydrogen bond, formed between a hydrogen atom and an electronegative atom covalently bound to each other, plays a pivotal role in stabilizing the secondary structure of proteins and is crucial for maintaining overall protein stability[32]. The quantification of intermolecular hydrogen bonds between the protein and the ligand at specific positions is computed through the analysis of MD simulation trajectories. The primary objective is to

assess the structural rigidity of the protein. The MD simulation, spanning 100 ns, allows for the continuous monitoring of the number of hydrogen bonds formed at each time point.

MM- GBSA- Binding free energy analysis

The determination of binding energy holds paramount importance in evaluating the structural and energetic attributes of protein complexes. Assessing the inhibitory potential of a ligand within the catalytic region is directly correlated with the overall binding free energy of the complex. Consequently, the calculation of binding free energy stands out as a pivotal factor in computational methodologies. In this study, the analysis of binding free energy was conducted employing the MM-GBSA (Molecular Mechanics with Generalized Born and Surface Area Solvation) technique within the Schrödinger Prime software. The estimation encompassed various protein complexes, including the Ligand-Receptor complex (RL), free ligand (L), and free receptor (R), as determined by the following equation,

$$\Delta G_{bind} = \Delta G_{RL} - [\Delta G_R + \Delta G_L]$$

$$\Delta E_{mm} = \Delta E_{bonding} + \Delta E_{vdW} + \Delta E_{ele}$$

Where ΔE_{vdW}, ΔE_{ele} and ΔG_{bind} are Van der waals, electrostatics protions, and bonded energy respectively[37].

Free energy decomposition was estimated to understand individual residue contributions to the intermolecular interaction[32]. To calculate the decomposition factors, the binding free energies (ΔE_{vdW}, ΔE_{ele}, ΔG_{bind}, *etc*.) are then broken down into per residual energy parameters. The raw data required for free energy decomposition analysis was obtained from the MM-GBSA output data.

Results

Overlapping Targets

In this study, an extensive retrieval of malarial and two *N*-alkylamides targets was executed using online tools including Gene Cards, OMIM, Swiss target prediction, and Super-PRED. After eliminating duplicates from each dataset, we individually compiled malarial targets and compounds-related targets, resulting in the identification of 2506 malarial targets and 248 phytocompound targets (Fig. 1). The Venn diagram, generated using the Venny online tool, revealed an overlap of 77 gene targets between the two datasets. These common targets form the basis for further analysis, providing a foundation for unravelling the intricate molecular interactions between malarial targets and phytocompounds.

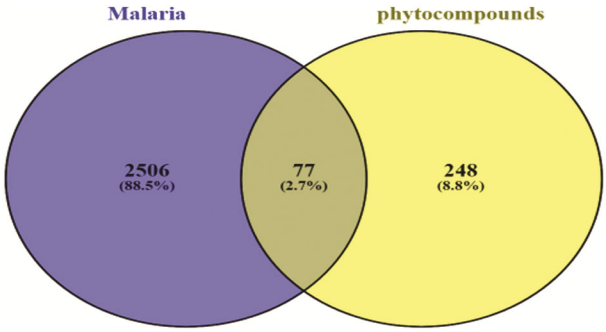

Fig. 1 — The Venn diagram showing intersection of disease and phytochemical targets

Table 1 — Top 5 key targets with node degree score

Target name	Gene symbol	Score	Betweenness Centrality
MMP9	29	29	0.0787037
SRC	27	27	0
TLR4	26	26	0
EGFR	26	26	0.037037
PTGS2	23	23	0

Construction and analysis of the compound-target-disease network

In our study, we conducted a node degree analysis to identify the top 5 key targets crucial for drug discovery. Table 1 presents a comprehensive overview of these targets, encompassing gene symbols, scores, and betweenness centrality values. Notably, MMP9 emerged as the most prominent target, reflecting a high node degree score of 29 and a betweenness centrality of 0.0787037. MMP9's pivotal role in extracellular matrix remodelling underscores its potential significance as a primary target for drug intervention.

Following MMP9, SRC, TLR4, EGFR, and PTGS2 also surfaced as noteworthy targets, each demonstrating substantial node degree scores and betweenness centrality values. SRC, a key player in cell signaling, and TLR4, integral to the innate immune system, hold promise as critical nodes in the drug discovery network. Furthermore, EGFR, a well-established therapeutic target in cancer, and PTGS2, associated with inflammation and pain, contribute to the multifaceted repertoire of potential drug targets (Table 1). Further, we performed a comprehensive approach to analyze the Compound-Target-Disease network, utilizing 77 overlapping targets to construct a "Protein-Protein Interaction" (PPI) network through

StringDB. The resulting PPI network comprised of 77 nodes and 293 edges, each delineating the intricate relationships between the two *N*-alkylamides such as Spilanthol and UDA and disease targets (malaria) (Fig. 2). The network's average node degree, a key metric indicative of the connectivity of nodes, was calculated at 7.61, providing a nuanced understanding of the interplay within the system (Fig. 3).

To further elucidate the core targets within the network, the "protein-protein interaction" (PPI) network was exported as a TSV file format and imported into Cytoscape software. By using the degree method, the identification of the top 10 core targets was accomplished, comprising 10 nodes and 41 edges. This prioritization sheds light on the most central elements within the network, offering valuable insights into potential key players in the antimalarial efficacy of Spilanthol and UDA. These findings not only contribute to our understanding of the intricate interactions within the Compound-Target-Disease network but also provide a foundation for targeted drug design and therapeutic interventions in the realm of antimalarial research.

The identification and subsequent ranking of five pivotal target genes were carried out in accordance with a descending order of node degree scores was reported[33]. The ranked targets, from highest to lowest node degree scores, include MMP9 (29), SRC (27), TLR4 (26), EGFR (26), and PTGS2 (23) (Fig. 4).

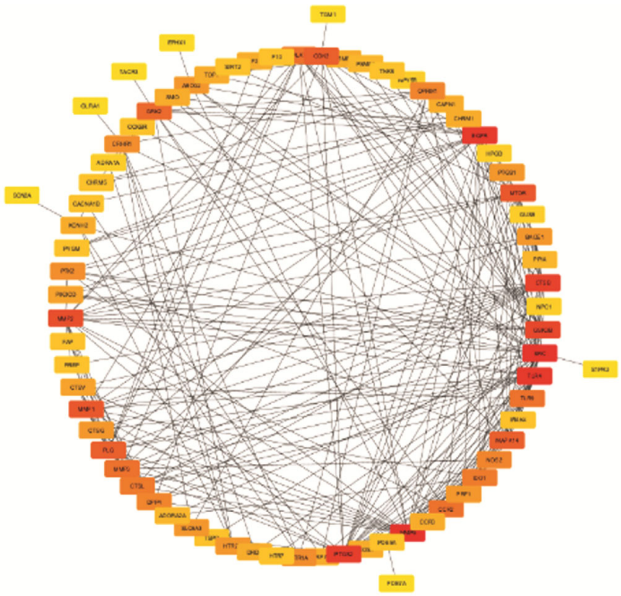

Fig. 3 — The key malaria targets of Spilanthol and UDA determined through topology analysis

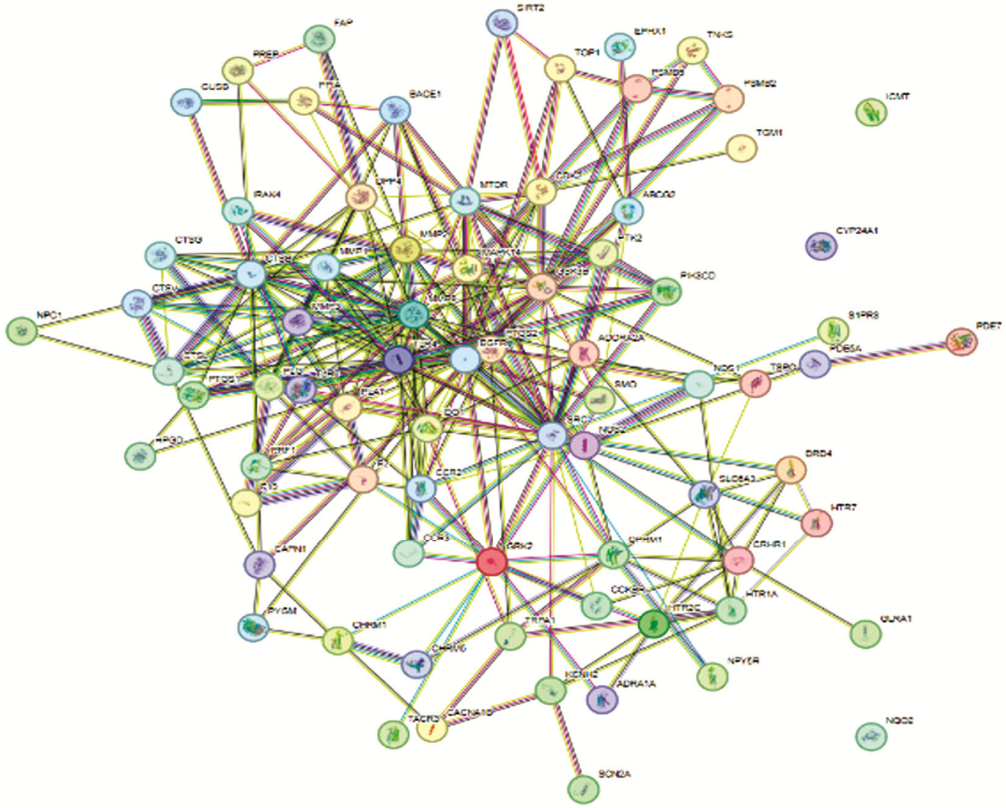

Fig. 2 — The PPI network of the 77 common targets between malaria and phytochemicals

Further, the ranking of key genes was determined based on their degree score and Betweenness centrality. Then, the resulting order of these crucial genes is presented in (Table 2). It encapsulates the outcomes of a pathway enrichment analysis, unveiling key molecular contexts associated with the dataset under scrutiny. The "Neuroactive ligand-receptor interaction" pathway (hsa04080) emerges as a focal point, exhibiting a substantial gene ratio of 19 out of 71, coupled with remarkably low p-values (1.42964E-10) and q-values (1.80587E-08). Similarly, the "Calcium signaling pathway" (hsa04020) and "Proteoglycans in cancer" (hsa05205) demonstrate significant enrichment, featuring gene ratios of 12 out of 71 and 11 out of 71, alongside low p-values (8.07843E-07, 1.22196E-06) and q-values (3.68372E-05). Other pathways, such as "Relaxin signaling pathway" (hsa04926), "Prostate cancer" (hsa05215), and "Endocrine resistance" (hsa01522), exhibit notable gene ratios and statistical significance. Additional pathways, including "Lipid and atherosclerosis" (hsa05417), "Fluid shear stress and atherosclerosis" (hsa05418), "Bladder cancer" (hsa05219), and "ErbB signaling pathway" (hsa04012), contribute to a comprehensive comprehension of the molecular underpinnings associated with the dataset, fostering a deeper insight into potential biological processes and pathways implicated in the analyzed data.

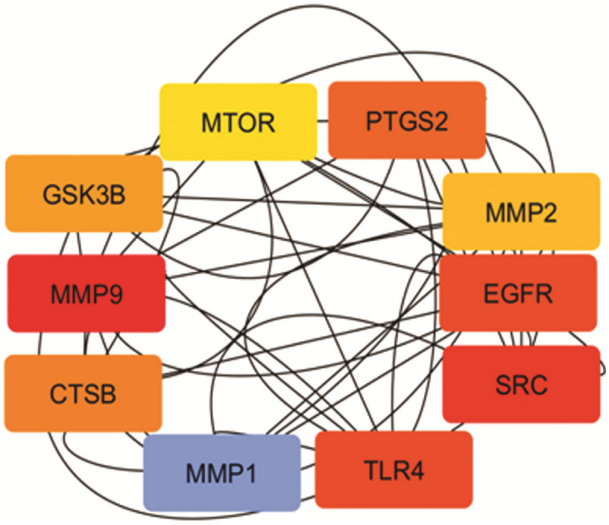

Fig. 4 — A network of top 10 key malaria targets of Spilanthol and UDA ranked based on node degree score

GO and KEGG pathway enrichment analysis

Utilizing the SRPLOT online tool, we conducted a comprehensive “Gene Ontology” (GO) and “Kyoto Encyclopedia of Genes and Genomes” (KEGG) pathway enrichment analysis, revealing a total of 1481 enriched GO terms ($P< 0.01$)[34]. These GO terms were distributed across “biological processes” (BP), “cellular components” (CC), and “molecular functions” (MF), yielding 1260, 100, and 121 terms, respectively. The top 10 GO terms, ranked based on *p*-values for BP, CC, and MF, were visually represented in a histogram, encompassing pivotal biological processes such as extracellular matrix disassembly, response of multicellular organisms to stress and G protein-coupled receptor signaling pathway coupled to cyclic nucleotide second messenger. Simultaneously, KEGG pathway enrichment analyses, employing a screening criteria of $P< 0.01$, identified 217 pathways (Fig. 5A). The subsequent construction of a bubble diagram (Fig. 5B) highlighting the top 10 enriched pathways unveiled a significant "target-pathway" network, offering comprehensive insights into potential molecular mechanisms associated with the analyzed dataset (Fig. 5B). In the constructed network, circle size corresponds to the number of genes correlated within the pathways, while colour signifies the p-value, with red denoting smaller values and blue

Table 2 — Top 10 KEGG pathways ranked based on *p*-value

ID	Description	Gene Ratio	*p*-value	*q*-value	Count
hsa04080	Neuroactive ligand - receptor interaction	19/71	1.42964E-10	1.80587E-08	19
hsa04020	Calcium signaling pathway	12/71	8.07843E-07	3.68372E-05	12
hsa05205	Proteoglycans in cancer	11/71	1.22196E-06	3.68372E-05	11
hsa04926	Relaxin signaling pathway	9/71	1.42542E-06	3.68372E-05	9
hsa05215	Prostate cancer	8/71	1.61797E-06	3.68372E-05	8
hsa01522	Endocrine resistance	8/71	1.74977E-06	3.68372E-05	8
hsa05417	Lipid and atherosclerosis	10/71	1.38777E-05	0.000250425	10
hsa05418	Fluid shear stress and atherosclerosis	8/71	2.36345E-05	0.000343776	8
hsa05219	Bladder cancer	5/71	2.4494E-05	0.000343776	5
hsa04012	ErbB signaling pathway	6/71	8.54555E-05	0.001079438	6

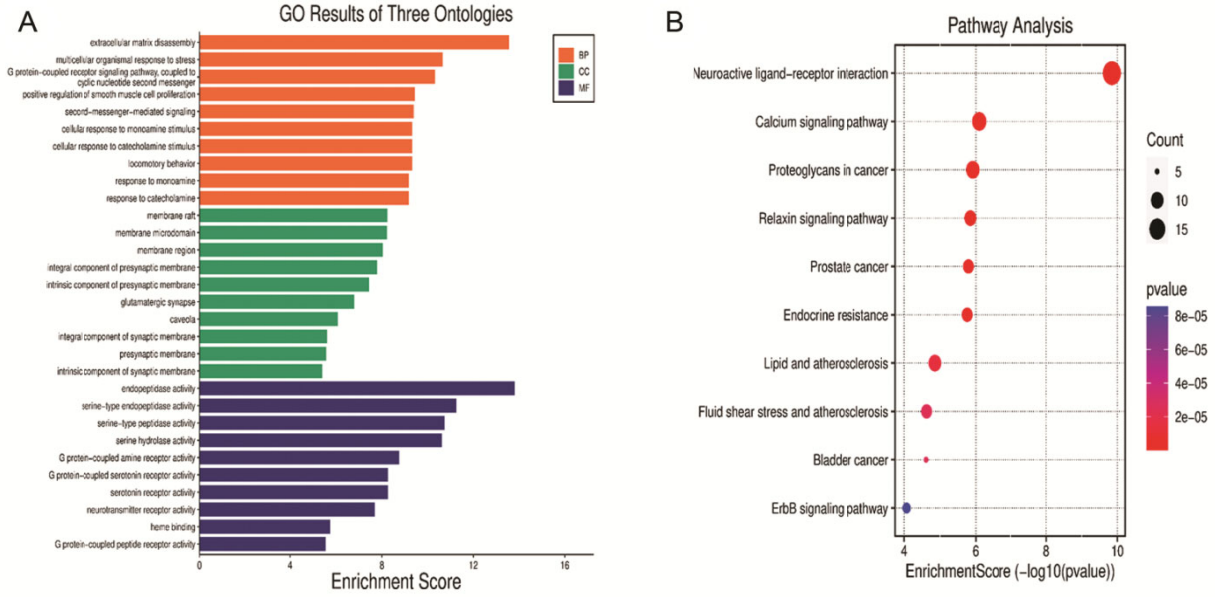

Fig. 5 — (A) The GO terms associated with common targets between malaria and phytochemicals; and (B) KEGG pathways associated with common targets between malaria and phytochemicals

indicating larger values[35,36]. The network prominently features key pathways, notably the Neuroactive ligand-receptor interaction (hsa04080), Calcium signaling pathway (hsa04020), Relaxin signaling pathway (hsa04926), and ErbB signaling pathway (hsa04012) collectively unveil noteworthy molecular interactions within the examined dataset. These findings contribute to a nuanced understanding of the functional landscape and pathway interactions, underscoring the utility of integrative bioinformatics analyses in elucidating the biological underpinnings of complex datasets.

Molecular docking verification and ADMET Profiling

In this investigation, molecular docking analyses were conducted utilizing the AutoDock Vina algorithm to explore the interactions between two potent *N*-alkylamides, namely Spilanthol and UDA, and crucial targets associated with malaria treatment, encompassing TLR4, PTGS2, MMP9, SRC, and EGFR. The binding affinity energy, crucial for gauging interaction strength, was calculated, with a lower binding affinity value indicating a more robust and stable complex formation. The results underscored PTGS2 as a notable target, exhibiting a smaller binding affinity with Spilanthol (-6.5 Kcal/mol) and UDA (-6.1 Kcal/mol), prompting the selection of both complexes for further analysis *via* Molecular Dynamics (MD) simulation to identify the most stable complex.

Subsequently, the visualization of the 3D docked structure was accomplished using the Chimera 1.17.3 tool (https://www.cgl.ucsf.edu/chimera/), while the Discovery Studio 2021 Client tool facilitated the retrieval of 2D interaction details for the docked complexes. The results highlights the specific binding residues involved in the interaction between Spilanthol and PTGS2 (amino acids ALA (202), GLN (203), HIS (388), and HIS (207)) and between UDA and PTGS2 (amino acids ARG (120), TYR (355), LEU (352), and VAL (116) (Fig. 6). The color-coded representation in the figures delineates vander waals interactions in green and alkyl interactions in pink, providing a comprehensive insight into the nature and strength of the molecular interactions at the binding site between the ligands and the PTGS2 target protein.

ADMET analysis was performed using SwissADME and ProTox-II online tool. Table 3 describes the ADMET profiling of the *N*-alkylamides, Spilanthol and UDA. This reveals several key pharmacokinetic and safety attributes which are critical for drug development. Both compounds exhibit high “gastrointestinal (GI) absorption” and permeability across the “blood-brain barrier” (BBB), indicating their potential efficacy in systemic circulation and central nervous system penetration. Importantly, they are not substrates for P-glycoprotein (P-gp), a transporter associated with drug efflux, which could enhance their bioavailability. In terms of cytochrome P450 (CYP) inhibition, both Spilanthol

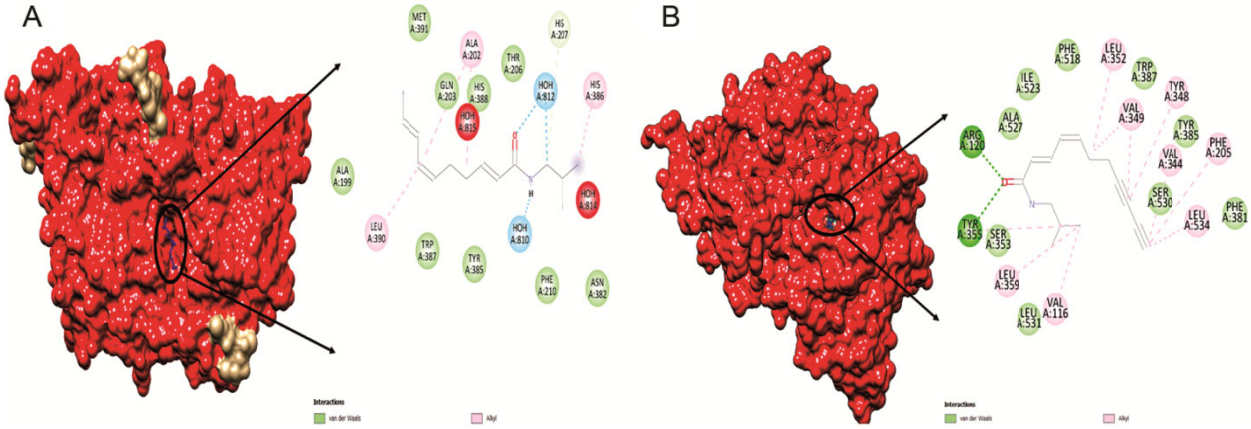

Fig. 6 — (A) 3D and 2D representation of PTGS2-Spilanthol interaction after docking; and (B) 3D and 2D representation of PTGS2-UDA interaction after docking

Table 3 — ADMET profiling of compounds

ADMET Profiling	Spilanthol	UDA
GI absorption	High	High
BBB permeant	Yes	Yes
P-gp substrate	No	No
CYP1A2 inhibitor	Yes	Yes
CYP2C19 inhibitor	No	No
CYP2C9 inhibitor	No	No
CYP2D6 inhibitor	No	No
CYP3A4 inhibitor	No	No
LD_{50}	4378 mg/kg	2000 mg/kg

and UDA show inhibitory effects on CYP1A2, suggesting potential interactions with drugs metabolized by this enzyme. However, they do not exhibit inhibitory effects on other major CYP isoforms (CYP2C19, CYP2C9, CYP2D6, and CYP3A4), minimizing concerns regarding drug-drug interactions.

Moreover, the LD50 values of Spilanthol (4378mg/kg) and UDA (2000mg/kg) suggest a relatively low acute toxicity, indicating a wide safety margin. In terms of hepatotoxicity and various toxicity tests (reverse mutation AMES test, carcinogenicity, mutagenicity, and cytotoxicity), both compounds exhibit inactivity, further supporting their favourable safety profile. These ADMET properties collectively position Spilanthol and UDA as promising candidates for further drug development, emphasizing their potential therapeutic utility with minimized risks of adverse effects.

Molecular dynamic simulation analysis

Based on the outcomes of molecular docking, the PTGS2-ligand complexes with the most favorable binding affinities for Spilanthol and UDA were identified and subjected to Molecular Dynamics (MD) simulations (Fig. 7). The analysis focused on evaluating the Root Mean Square Deviation (RMSD) of the docked structures, specifically tracking the structural deviations over the simulation trajectory, to gain insights into the stability and dynamics of the Spilanthol and UDA interactions with the PTGS2 target. The RMSD (PTGS2 docked with Spilanthol) of the protein represented on the left side of the RMSD plot, indicates that the C-α atoms reach their maximum deviation at 48 ns. The plot reveals fluctuations in protein RMSD for C-α atoms ranging from 0.8 Å to 2.8 Å, a range considered within normal fluctuation limits. It is noteworthy that these fluctuations remain below the threshold of 3 Å, signifying that the protein experienced typical and acceptable conformational changes during the MD simulation. Notably, beyond 80 ns, the substantial fluctuations in protein RMSD diminish, reaching convergence, indicating a stabilized and equilibrated state of the protein system, as observed in prior studies[37].

In Figure 7A, the ligand RMSD is depicted on the right side of the plot, offering insights into the stability of the ligand throughout the simulation. Notably, Spilanthol demonstrates minimal deviation from the protein RMSD observed during the MD simulation, implying that the ligand has not diffused substantially from its initial binding site, maintaining a stable interaction profile during the MD simulation. Figure 7B represents the protein RMSF plot, where Spilanthol shows C-α and B-factor values of less than 8 Å with residue index. Contrasting to the Spilanthol-PTGS2 complex's RMSD plot, the RMSD plot of PTGS2 docked with UDA reveals fluctuations exceeding 3 Å (Fig. 7C), indicating considerable

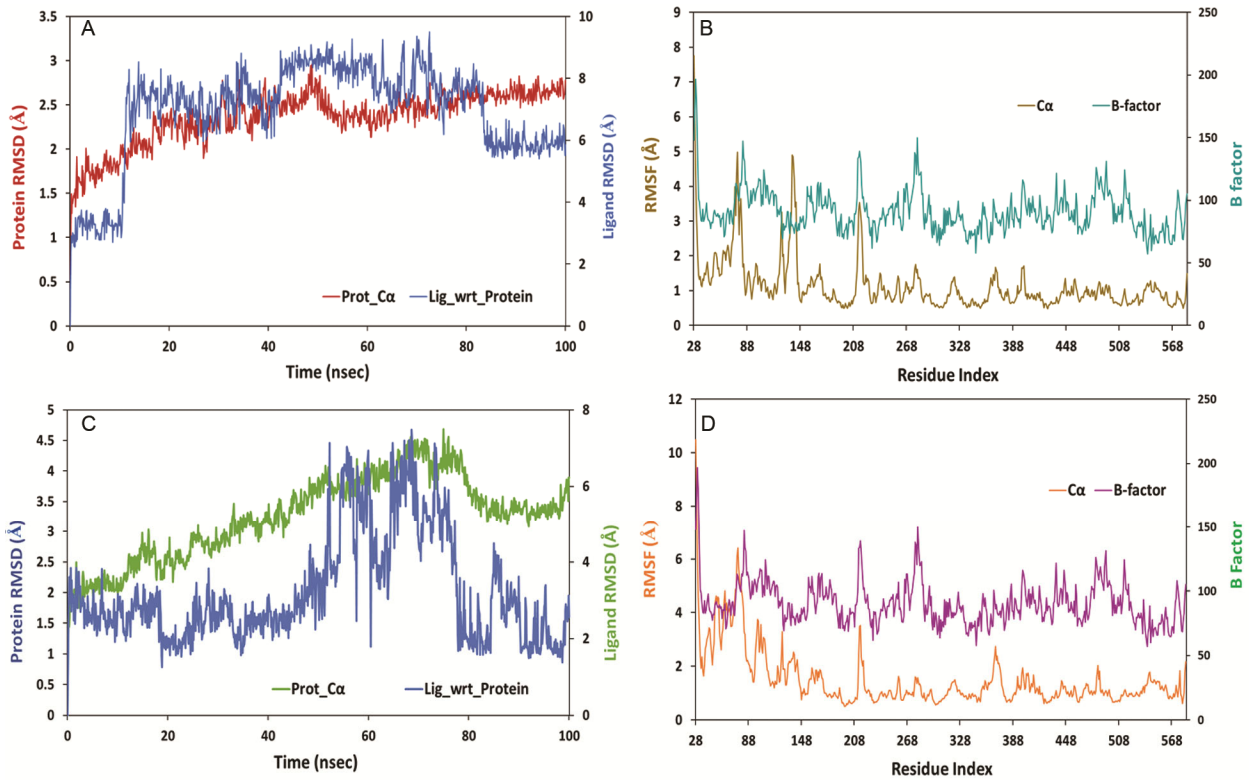

Fig. 7 — (A) The RMSD plot of PTGS2-Spilanthol complex during MD simulation; (B) The RMSF plot of PTGS2-Spilanthol complex during MD simulation; (C) The RMSD plot of PTGS2-UDA complex during MD simulation; and (D) The RMSF plot of PTGS2-UDA complex during MD simulation

deviations and suggesting a departure from the anticipated stability observed in the Spilanthol-PTGS2 complex. The ligand RMSD plot also reveals substantial deviations from the protein RMSD, indicating that the ligand has diffused away from its initial binding site, further suggesting instability compared to the Spilanthol-PTGS2 complex, as outlined in previous analyses[38]. Figure 7D represents the protein RMSF plot, where UDA shows C-α and B-factor values greater than 10.

The comprehensive assessment of overall RMSD fluctuations, coupled with the minimal deviation difference between protein RMSD and ligand RMSD[39], underscores the high stability of the selected complex. Specifically, the Spilanthol-PTGS2 docked complex exhibits greater stability compared to the UDA-PTGS2 docked complex. These findings provide a nuanced understanding of the protein's dynamic behavior, emphasizing the specific residues involved in ligand interactions and highlighting the structural elements maintaining stability throughout the simulation period. Figures 8A and 8B illustrate the dynamic interplay between the ligand and protein throughout the simulation. The Y-axis illustrates the interaction fraction, while the X-axis corresponds to the amino acid residues within the binding site. The classification of protein-ligand contacts encompasses four types: Hydrogen bonds (green), hydrophobic contacts (purple), ionic interactions (pink), and water bridges (blue). Of particular significance, hydrogen bonds play a pivotal role in ligand binding dynamics, aligning with established criteria[40]. The geometric standards for protein-ligand H-bonding include a distance of 2.5 Å between the donor and acceptor atoms, with a donor angle of $\geq 120°$ and an acceptor angle of $\geq 90°$, contributing to the robust understanding of the intricate intermolecular interactions governing stability and specificity.

In Figure 8A, the H-bonds exhibit a substantial interaction fraction exceeding 0.5 (50%), notably prevalent in GLN(202) (51%) and HIS(388) (80%) amino acid residues, indicating persistent interactions over 50% of the simulation duration. Moreover, water bridges play a significant role in mediating protein-ligand interactions, displaying heightened interaction fractions, particularly in GLN(202) and HIS(388) residues. In contrast, Figure 8B portrays fewer H-bonds but an increased occurrence of hydrophobic

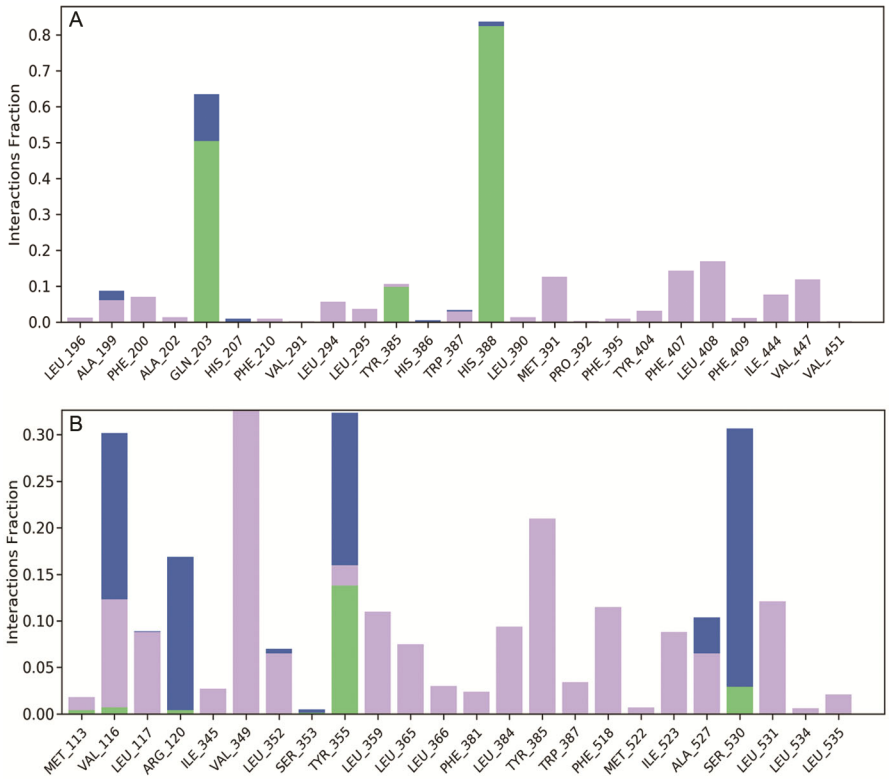

Fig. 8 — (A) Histogram of protein-ligand contacts established between PTGS2 and Spilanthol during the simulation; and (B) Histogram of protein-ligand contacts established between PTGS2 and UDA during the simulation (Green, blue and violet colour bars represents hydrogen bond, water bridges and hydrophobic interactions, respectively)

contacts, accompanied by extensive water bridges involving VAL_116 and ALA_527 residues. The histogram plot further underscores interaction fractions surpassing 0.3 (30%) simulation time for any given residue, highlighting prolonged interaction fractions observed in residues HIS(388) and GLN(203) within the Spilanthol-PTGS2 complex. These findings are corroborated through residue 2D interaction analysis. In Figure 9A, HIS(388) and GLN(203) residues are prominently engaged, accounting for 82% and 47% of the simulation time, respectively, within the ligand binding site. This underscores their sustained involvement in the Spilanthol-PTGS2 complex over the simulation. Figure 9B further substantiates these observations, illustrating the consistent positioning of HIS(388) throughout the simulation period, emphasizing its stability and role within the complex.

The average bond formation events for Spilanthol during the simulation were observed to be 3 (Fig. 9C). HIS(388) exhibited prolonged contacts, spanning from 13 to 82 sec, with additional interactions between 85 to 90 sec and 95 to 100 sec. Additionally, TYR(385) displayed its longest contact period between 0 to 10 sec, while GLN(203) demonstrated varied contact intervals. Similarly, for UDA, the average bond formation events were 3 during the simulation (Fig. 9D). Noteworthy contacts included Ser 530, spanning from 7 to 35 sec and again from 81 to 88 sec, and TYR(355) exhibited prolonged interactions between 18 to 44 sec, 77 to 83 sec, and 90 to 99 sec. VAL(349) had contact periods from 0 to 12 sec, while VAL(116) demonstrated interactions between 45 to 52 sec and 96 to 100 sec. ARG(120) also displayed contacts between 43 to 52 sec. This detailed analysis provides insights into the dynamic interactions between the ligands and target residues over the simulation period.

H-bond monitoring during 100 ns MD simulation

The intermolecular H-bond interactions between Spilanthol and UDA with target PTGS2 were analysed and validated by H-Bond monitored during MD simulation. In molecular dynamics (MD) simulations, hydrogen bonds play a crucial role in determining the structure, stability, and dynamics of biomolecules such as proteins, nucleic acids, and other macromolecules[41].

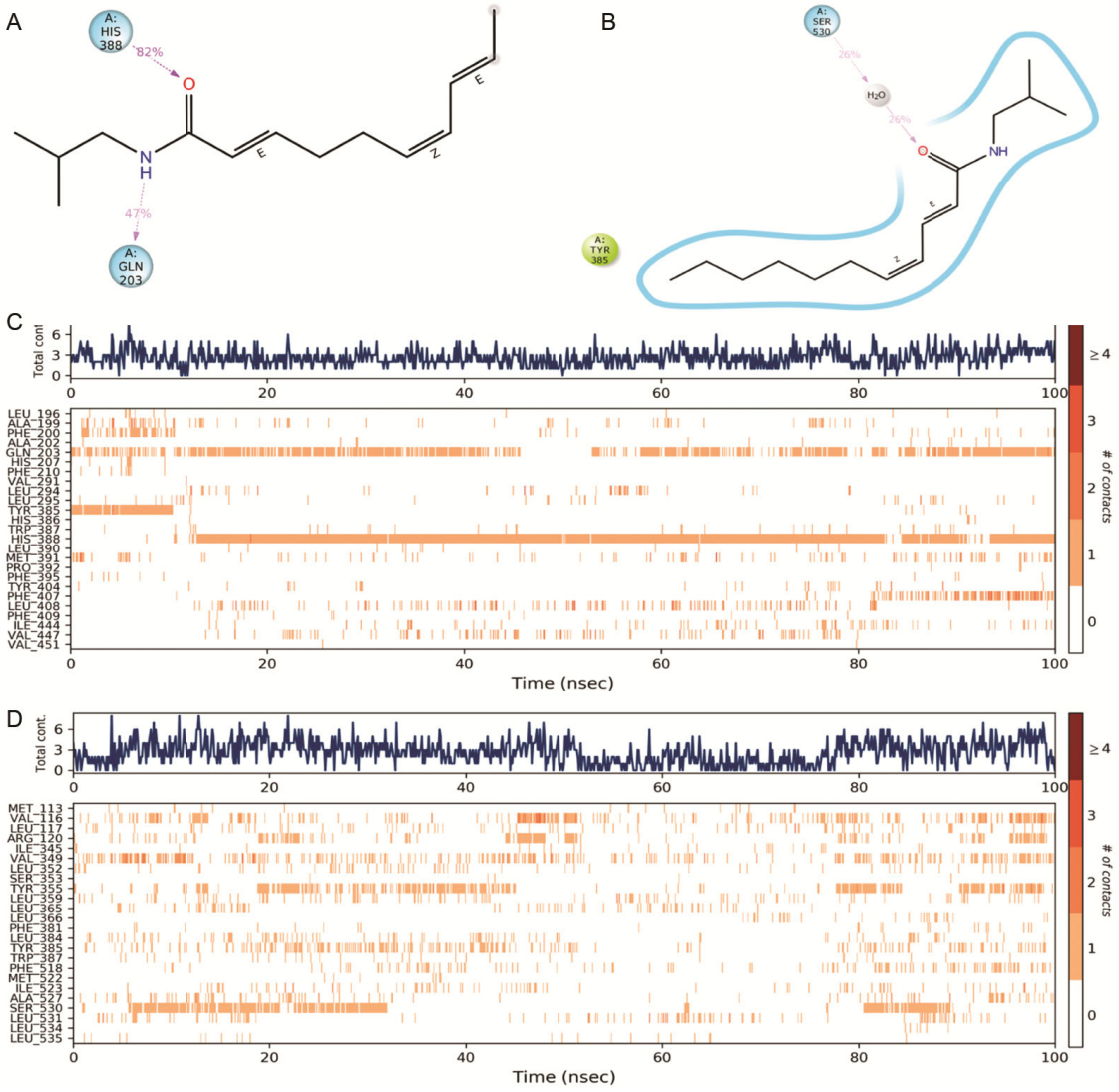

Fig. 9 — 2D representation and timeline representation of fraction of contacts made by Spilanthol and UDA with PTGS2; (A) Spilanthol with the residues of PTGS2; (B) UDA with the residues of PTGS2 during MD simulation. (The purple arrows represent hydrogen bonds); (C) Timeline representation of Spilanthol during a 100 ns MD simulation; and (D) Timeline representation of UDA during a 100 ns MD simulation

During the molecular dynamics (MD) simulation, the Spilanthol-PTGS2 complex (Fig. 10A) exhibited a dynamic pattern of hydrogen bond formation, reaching a peak of 4 bonds within the initial 12 ns. Subsequently, a gradual decline to 3 hydrogen bonds occurred by 32 ns, stabilizing at 2 hydrogen bonds from 35 ns to 100 ns. Despite a minor fluctuation with 3 hydrogen bonds at 78 ns, the overall equilibrium and stability of the complex remained unaffected. This observation aligns well with the interaction histograms seen previously, depicting that more than 50% of hydrogen bonds were sustained throughout the MD simulation, indicating their stabilization after 35 ns with minimal fluctuation.

Contrastingly, the UDA-PTGS2 complex (Fig. 10B) presented a diverse behaviour over the 100 ns simulation. It initially demonstrated a substantial number of hydrogen bonds (1-2) within the first 20 ns, increasing to 3 hydrogen bonds between 43 ns and 62 ns. However, the simulation revealed a considerable fluctuation in the number of hydrogen bonds, suggesting weak hydrogen bonding and overall instability in the protein-ligand complex. This observation is reinforced by Figure 8B, where the histogram of protein-ligand contacts between PTGS2 and UDA illustrates only 12% hydrogen bonding and a predominant percentage of interactions involving water bridges. This nuanced comparison sheds light

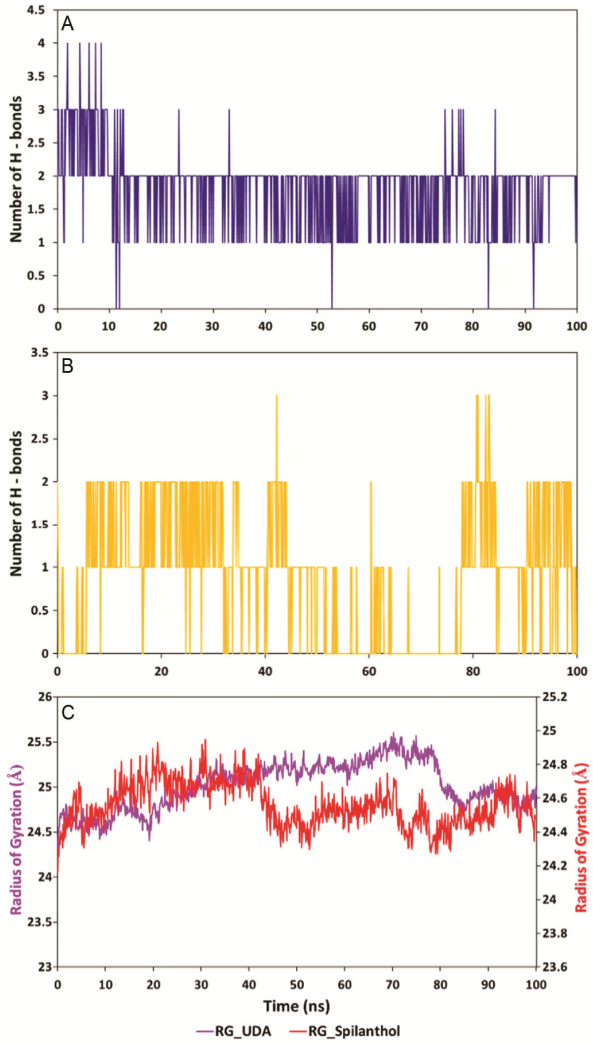

Fig. 10 — H-bond monitoring during 100 ns; (A) Spilanthol-PTGS2 complex, (B) UDA – PTGS2 complex; and (C) Radius of Gyration plot from MD simulation for both spilanthol and UDA

on the divergent behaviour of the two complexes, emphasizing the stability of the Spilanthol-PTGS2 complex in terms of sustained hydrogen bonds throughout the simulation.

Radius of Gyration (Å)

In our analysis, the parameter of radius of gyration (Rg) serves as a critical metric for assessing the stability of protein folding. A consistent Rg value signifies stable folding, while fluctuations over time indicate instability in the folding process[42]. As depicted in Figure 10C, the Rg profile for Spilanthol (RG_Spilanthol) maintains a remarkably stable range between 24.2 Å and 24.7 Å throughout the entire 100 ns simulation. This observation underscores the stable folding of the protein induced by Spilanthol. Conversely, the Rg profile for UDA (RG_UDA) exhibits notable fluctuations over the entire simulation period, indicating a comparatively less stable folding in the UDA complex.

Furthermore, the graphical representation illustrates the dynamic fluctuations in both Spilanthol and UDA complexes. Intriguingly, these fluctuations in both phytocompounds tend to linearized after 80 ns, suggesting that the protein complex attains a state of increased stability beyond this point in the simulation. This critical analysis provides valuable insights into the temporal dynamics of protein folding stability induced by Spilanthol and UDA, contributing to a comprehensive understanding of their impact on the protein structure.

Analysis of binding free energy by MM-GBSA

The assessment of ligand persistence in binding to the target protein structure involves a thorough examination of binding free energy measurements, as outlined in (Table 4). This table presents diverse energy factors, measured in kilocalories per mole (Kcal/mol), for two ligands: UDA and Spilanthol. These energy factors signify the energetics associated with the interaction between the ligands and the target molecule or receptor.

The comprehensive binding free energy values serve as indicators of the thermodynamic favorability of ligand binding to the target, with lower values generally indicating stronger binding affinity. Both Spilanthol and UDA complexes, particularly with PTGS2, demonstrate exemplary binding energy in the docking process. The establishment of covalent bonds between the protein and ligand ensures a robust, stable, and enduring connection. Specifically, Spilanthol exhibits a notable ΔGbind_Covalent energy of 1.833, surpassing UDA with a value of 1.576. This discrepancy highlights the high degree of electron sharing and, consequently, the enhanced stability conferred by Spilanthol in forming covalent bonds within the protein-ligand complex.

The significance of hydrogen bonding in protein-ligand interactions cannot be overstated, as it profoundly influences binding affinity, specificity, and overall complex stability. Negative values, as observed with spilanthol and UDA, signify favorable hydrogen bonding, with spilanthol exhibiting an

Table 4 — MM-GBSA free-energy calculation for spilanthol and UDA

Energy factors (Kcal/mol)	UDA		Spilanthol	
	Mean	Standard deviation	Mean	Standard deviation
ΔG_{bind}	-51.267	5.927	-50.385	9.302
ΔG_{bind}_Coulomb	-3.792	3.915	-16.839	3.503
ΔG_{bind}_Covalent	1.576	1.049	1.833	1.168
ΔG_{bind}_Hbond	-0.178	0.240	-0.825	0.288
ΔG_{bind}_Lipo	-23.678	2.074	-19.200	3.527
ΔG_{bind}_vdW	-46.506	1.436	-36.823	3.005

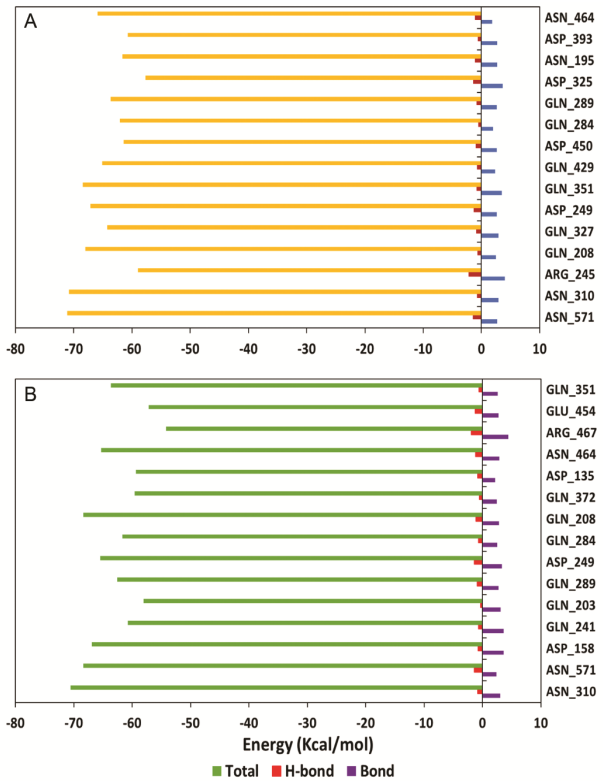

Fig. 11 — Binding free energy comparison for (A) Spilanthol – PTGS2 complex; (B) UDA – PTGS2 complex

exceptional ΔGbind_H-bond of -0.825 and UDA showing a commendable value of -0.178. In summary, spilanthol demonstrates robust and stable protein-ligand bonding during the docking process.

The binding free energy estimation during the simulation period was assessed using the MM-GBSA method . Figure 11A illustrates that the total free energy for the spilanthol-PTGS2 docked complex ranges from -55 Kcal/mol to -73 Kcal/mol, showcasing excellent total energy and hydrogen bonding stability. Similarly,Figure 11B exhibits a total free energy range from -50 Kcal/mol to -73 Kcal/mol for the UDA-PTGS2 docked structure. These findings underscore the favorable and stable energetics of both complexes during the MD simulation, further reinforcing their potential as promising candidates for continued investigation.

Discussion

The recent strides in drug development within computational biology have significantly advanced the identification and modulation of crucial drugs. Despite these achievements, certain diseases, including malaria, pose persistent challenges in drug development. Malaria, characterized as a parasitic disease with substantial public health implications, remains a formidable target for therapeutic interventions. This groundbreaking study introduces a comprehensive computational approach to assess the potential of N-alkylamides, specifically Spilanthol and UDA, as inhibitors for novel malaria-associated targets. These secondary metabolites, predominantly found in herbaceous plants, have garnered attention for their pharmacological effects on various diseases[11]. The amalgamation of "network pharmacology", "molecular docking", and "molecular dynamics simulations" offers a nuanced exploration of the interactions between these drugs and malarial target genes, shedding light on their inhibitory capacities.

Traditionally, phytochemicals derived from plants have been harnessed for centuries in the treatment of malaria. Earlier studies have indicated the efficacy of *Spilanthes acmella* and its specific *N*-alkylamides, Spilanthol and UDA, against *Plasmodium falciparum*. *In vivo* experiments involving mice infected with *P. yoelii yoelii* 17XNL revealed a significant reduction in parasitemia in mice blood, demonstrating their potential as anti-malarial agents[43]. Additionally, both Spilanthol and UDA have exhibited biotherapeutic potential against the erythrocytic stages of the malaria parasite[8].

Similarly, the current study establishes Spilanthol as an effective inhibitor against the PTGS2 target. Network pharmacology identified key target genes based on their node degree score and betweenness

centrality properties, with MMP9 emerging as the primary target with a node degree of 29. Notably, the most effective target gene had a node degree value of 23, challenging the assumption that the gene with the highest node degree is always the most effective target. Molecular docking results revealed that among the top targets, PTGS2 exhibited a lower binding affinity with Spilanthol (-6.5 Kcal/mol) and UDA (-6.1 Kcal/mol), emphasizing its significance as a target for inhibitory activity. Previous research on Spilanthol from *Acmella oleracea* explored its anti-tumor activity against gastric cancer, targeting JAK1 (binding affinity: -8.38 kJ/mol) and JAK2 (binding affinity: -9.71 kJ/mol) proteins. Furthermore, the prevalence of van der Waals forces between Spilanthol and JAK proteins indicated structural stability[44]. The majority of amino acid interactions between PTGS2 and Spilanthol (amino acid residues: HIS 388, GLN 203) were attributed to Vander Waals forces, emphasizing their role in structural stability.

The assessment of drugs' ability to traverse physiological barriers and their pharmacokinetic properties provides crucial insights into their efficacy. These aspects are comprehensively examined through ADMET studies. Both Spilanthol and UDA demonstrated high "gastrointestinal absorption" and "blood-brain barrier" permeability. A notable FDA-approved malaria drug, Chloroquine, is commonly prescribed for treatment. In comparison, Spilanthol and UDA exhibited no toxicity in the AMES test, whereas, Chloroquine demonstrated significant toxicity (Probability - 0.9106) (https://go.drugbank.com/drugs/DB00608). Moreover, they displayed no hepatotoxicity or carcinogenicity. During molecular dynamic simulation, the Spilanthol-PTGS2 complex exhibited greater stability than the UDA-PTGS2 complex, as indicated by factors inferred from RMSD and RMSF plots. The hydrogen bond analysis conducted over the 100 ns Molecular Dynamics (MD) simulation provides valuable insights into the stability of the complexes. The spilanthol-PTGS2 complex exhibits a sustained pattern of hydrogen bonds, indicative of stable interactions. Utilizing the radius of gyration (Rg) to evaluate protein folding stability in both spilanthol-PTGS2 and UDA-PTGS2 complexes, it is observed that the former maintains a consistent and stable Rg throughout the simulation, signifying robust protein folding. Conversely, UDA-PTGS2 experiences fluctuations in Rg, suggesting comparatively less stability. The eventual linearization of fluctuations post-80 ns indicates an attaining of stability, but the presence of fluctuating hydrogen bonds in UDA-PTGS2 implies weaker and less stable binding.

The MM-GBSA analysis further quantifies various energy factors contributing to ligand binding. Notably, Spilanthol demonstrates a higher ΔGbind_Covalent energy, indicating strong covalent bonding. Favorable ΔGbind_H-bond values for both compounds underscore the significant contributions of hydrogen bonding. Consistently lower ΔGbind, ΔGbind_Lipo, and ΔGbind_vdW values for Spilanthol compared to UDA suggest stronger and more stable binding interactions. This comprehensive analysis reinforces Spilanthol's superiority in terms of binding strength and stability, supporting its potential as a robust anti-malarial candidate. Our integrated computational analysis not only identifies promising inhibitors for malaria target genes but also establishes a foundation for further experimental validation and potential drug development endeavours in the pursuit of effective antimalarial agents.

Conclusion

This study utilized molecular docking, network pharmacology and molecular dynamics to investigate the potential of secondary metabolites, Spilanthol and UDA, for malaria treatment. Screening identified 77 common target genes, with MMP9, SRC, TLR4, EGFR, and PTGS2 selected as core targets. GO and KEGG pathway analysis revealed anti-malarial effects, inhibiting key pathways. Molecular docking highlighted strong affinity between Spilanthol and PTGS2, and ADMET profiling favoured Spilanthol for its excellent biocompatibility. Molecular dynamics indicated stability in the Spilanthol-PTGS2 complex, with a prolonged interaction fraction between residues HIS (388) and GLN(203). This comprehensive analysis provides profound insights into the potential therapeutic role of N-alkylamides against malarial targets, positioning both secondary metabolites as promising anti-malarial agents.

Acknowledgement

The authors express sincere appreciation to the Bioinformatics Lab facility of the Department of Biotechnology, PSG College of Technology, for providing essential support and resources for conducting this research.

Conflict of interest

All authors declare no conflict of interest.

References

1 Adams L, Afiadenyo M, Kwofie SK, Wilson MD, Kusi KA, Obiri-Yeboah D, Moane S & McKeon-Bennett M, *In silico* screening of phytochemicals from Dissotis rotundifolia against *Plasmodium falciparum* Dihydrofolate Reductase. *Phytomed Plus*, 3 (2023) 100447.

2 Saba N, Balwan WK & Mushtaq F, Burden of Malaria-A Journey Revisited. *Sch J App Med Sci*, 6 (2022) 934.

3 Wanzira H, Katamba H, Okullo AE, Agaba B, Kasule M, & Rubahika D, Factors associated with malaria parasitaemia among children under 5 years in Uganda: a secondary data analysis of the 2014 Malaria Indicator Survey dataset. *Malar J*, 16 (2017) 1.

4 Khalid M, Kayani SI, Jan F, Ullah A, Tang K. Biological activities of artemisinins beyond anti-malarial: a review. *Trop Plant Biol*, 12 (2019) 231.

5 Edison M, Jeeva JB, & Singh, M, Sequential analysis of erythrocyte aggregation in *P. falciparum* malaria with and without ASAQ therapy by optical signal and image analysis. *Indian J Biochem Biophys,* 60 (2023) 331.

6 Tse EG, Korsik M & Todd MH, The past, present and future of anti-malarial medicines. *Malar J*, 18 (2019) 1.

7 Cock IE, Selesho MI & Van Vuuren SF, A review of the traditional use of southern African medicinal plants for the treatment of malaria. *J Ethnopharmacol*, 245 (2019) 112176.

8 Rajendran R, Narashimman BS, Trivedi V & Chaturvedi R, Isolation and quantification of antimalarial N-alkylamides from flower-head derived *in vitro* callus cultures of *Spilanthes paniculata*. *J Biosci Bioeng*, 124 (2017) 99.

9 Kiguba R, Olsson S & Waitt C, Pharmacovigilance in low-and middle-income countries: a review with particular focus on Africa. *Br J Clin Pharmacol*, 89 (2023) 491.

10 Farha S, Gade R, Priya ML, Dwarampudi LP & Dhanapal SP, Phytochemical evaluation and anti-psoriatic activity of the ethanolic extract of the leaves of *Thespesia populnea*. *Indian J Biochem Biophys*, 60 (2023) 156.

11 Abdul Rahim R, Jayusman PA, Muhammad N, Mohamed N, Lim V, Ahmad NH, Mohamad S, Abdul Hamid ZA, Ahmad F, Mokhtar N & Shuid AN, Potential antioxidant and anti-inflammatory effects of spilanthes acmella and its health beneficial effects: a review, *Int. J. Environ Res Public Health*, 18 (2021) 3532.

12 Masoko, P. Phytochemical analysis, antioxidant and antibacterial properties of Spilanthes mauritiana used traditionally in Limpopo Province, South Africa. *J Evid Based Complement Altern Med*, 22 (2017) 936.

13 Daina A, Michielin O & Zoete V, SwissTarget Prediction: updated data and new features for efficient prediction of protein targets of small molecules. *Nucleic Acids Res*, 47 (2019) 357.

14 Gallo K, Goede A, Preissner R & Gohlke BO, SuperPred 3.0: drug classification and target prediction—a machine learning approach. *Nucleic Acids Res,* 50 (2022) 726.

15 Lin Y & Hu Z, Bioinformatics analysis of candidate genes involved in ethanol-induced microtia pathogenesis based on a human genome database: GeneCards. *Int J Pediatr Otorhinolaryngol*, 142 (2021) 110595.

16 Hamosh A, Amberger JS, Bocchini C, Scott AF & Rasmussen SA, Online mendelian inheritance in man (OMIM®): Victor McKusick's magnum opus. *Am J Med Genet A*, 185 (2021) 3259.

17 Szklarczyk D, Kirsch R, Koutrouli M, Nastou K, Mehryary F, Hachilif R, Gable AL, Fang T, Doncheva NT, Pyysalo S & Bork P, The STRING database in 2023: protein–protein association networks and functional enrichment analyses for any sequenced genome of interest. *Nucleic Acids Res*, 51 (2023) 638.

18 Hamdy H, Yang Y, Cheng C & Liu Q, Identification of Potential Hub Genes Related to Aflatoxin B1, Liver Fibrosis and Hepatocellular Carcinoma *via* Integrated Bioinformatics Analysis. *Biology*, 12 (2023) 205.

19 Li C, Hu J, Liu P, Li Q, Chen J, Cui Y, Zhou X, Xue B, Zhang X, Gao X & Zu X, A comprehensive evaluation of differentially expressed mRNAs and lncRNAs in cystitis glandularis with gene ontology, KEGG pathway, and ceRNA network analysis. *Transl Androl Urol*, 9 (2020) 232.

20 Reddy YV, Swiss ADME predictions of phytoconstituents present in Ocimum sanctum Linn. *J Pharmacogn Phytochem*, 12 (2023) 17.

21 Banerjee P & Ulker OC, Combinative ex vivo studies and in silico models ProTox-II for investigating the toxicity of chemicals used mainly in cosmetic products. *Toxicol mech methods*, 32 (2022) 548.

22 Che X, Liu Q & Zhang L, An accurate and universal protein-small molecule batch docking solution using Autodock Vina. *Results Eng*, 19 (2023) 101335.

23 Patel JR, Joshi HV, Shah UA & Patel JK, A review on computational software tools for drug design and discovery. *Indo Global J Pharm Sci*, 12 (2022) 53.

24 Goodsell DS, Zardeck C, Di Costanzo L, Duarte JM, Hudson BP, Persikova I & Burley SK, RCSB Protein Data Bank: Enabling biomedical research and drug discovery. *Protein Sci*, 29 (2020) 52.

25 Barber RD, Software to visualize proteins and perform structural alignments. *Curr Protoc*, 1 (2021) e292.

26 Eberhardt J, Santos-Martins D, Tillack AF & Forli S, AutoDock Vina 1.2. 0: New docking methods, expanded force field, and python bindings. *J Chem Inf Model*, 61 (2021) 3891.

27 Sengupta A, Li Z, Song LF, Li P & Merz Jr KM, Parameterization of monovalent ions for the OPC3, OPC, TIP3P-FB, and TIP4P-FB water models. *J Chem Inf Model*, 61 (2021) 869.

28 Simmonett AC & Brooks BR, A compression strategy for particle mesh Ewald theory. *J Chem Phys*, 154 (2021) 054112.

29 Robertson MJ & Skiniotis G, Development of OPLS-AA/M parameters for simulations of G protein-coupled receptors and other membrane proteins. *J Chem Theory Comput*, 18 (2022) 4482.

30 Gopinath P & Kathiravan MK, Docking studies and molecular dynamics simulation of triazole benzene sulfonamide derivatives with human carbonic anhydrase IX inhibition activity. *RSC Adv*, 11 (2021) 38079.

31 Parida PK, Paul D & Chakravorty D, The natural way forward: molecular dynamics simulation analysis of phytochemicals from Indian medicinal plants as potential inhibitors of SARS-CoV -2 target. *Phytother Res*, 34 (2020) 3420.

32 Ghahremanian S, Rashidi MM, Raeisi K & Toghraie D, Molecular dynamics simulation approach for discovering potential inhibitors against SARS-CoV-2: A structural review. *J Mol Liq*, 354 (2022) 11890.

33 Ma H, He Z, Chen J, Zhang X & Song P, Identifying of biomarkers associated with gastric cancer based on 11 topological analysis methods of CytoHubba. *Sci Rep*, 11 (2021) 1331.

34 Dai GP, Wang LP, Wen YQ, Ren XQ & Zuo SG, Identification of key genes for predicting colorectal cancer prognosis by integrated bioinformatics analysis. *Oncol Lett*, 19 (2020) 388.

35 Luo W, Deng J, He J, Yin L, You R, Zhang L, Shen J, Han Z, Xie F, He J & Guan Y, Integration of molecular docking, molecular dynamics and network pharmacology to explore the multi-target pharmacology of fenugreek against diabetes. *J Cell Mol Med*, 27 (2023) 1959.

36 Shi Y, Chen M, Zhao Z, Pan J & Huang S, Network pharmacology and molecular docking analyses of mechanisms underlying effects of the cyperirhizoma-chuanxiong rhizoma herb pair on depression. *Evid Based Complement Alternat Med*, 1 (2021) 5704578.

37 Wang J, Arantes PR, Bhattarai A, Hsu RV, Pawnikar S, Huang YMM & Miao Y, Gaussian accelerated molecular dynamics: Principles and applications. *Wiley Interdiscip Rev Comput Mol Sci*, 11 (2021) e1521.

38 Chikhale RV, Gupta VK, Eldesoky GE, Wabaidur SM, Patil SA & Islam MA, Identification of potential anti-TMPRSS2 natural products through homology modelling, virtual screening and molecular dynamics simulation studies. *J Biomol Struct Dyn*, 39 (2021) 6660.

39 Celik I & Tallei TE, A computational comparative analysis of the binding mechanism of molnupiravir's active metabolite to RNA-dependent RNA polymerase of wild-type and Delta subvariant AY. 4 of SARS-CoV-2. *J Cell Biochem*, 123 (2022) 807.

40 Rajasekhar S, Karuppasamy R & Chanda K, Exploration of potential inhibitors for tuberculosis *via* structure-based drug design, molecular docking, and molecular dynamics simulation studies. *J Comput Chem*, 42 (2021) 1736.

41 Çakmak Ş & Erdoğan T, Some bis (3-(4-nitrophenyl) acrylamide derivatives: Synthesis, characterization, DFT, antioxidant, antimicrobial properties, molecular docking and molecular dynamics simulation studies. *Indian J Biochem Biophys,* 60 (2023) 209.

42 Saffari-Chaleshtori J, Shafiee SM & Heidarian E, The effect of bilirubin on Bad, Bak, and Bim pro-apoptotic factors: A molecular dynamic simulation study. *Indian J Biochem Biophys,* 58 (2021) 236.

43 Elufioye TO, Habtemariam S & Adejare A, Chemistry and pharmacology of alkylamides from natural origin. *Rev Bras Farmacogn*, 30 (2020) 622.

44 Pinheiro MS, Moysés DA, Galucio NC, Santos WO, Pina JR, Oliveira LC, Silva SY, Silva SD, Frazão NF, Marinho PS & Novais AL, Cytotoxic and molecular evaluation of Spilanthol obtained from *Acmella oleracea* (L.) RK Jansen (jambu) in human gastric cancer cells. *Nat Prod Res*, 38 (2023) 1806.

45 Asir F, Oglak SC, Korak T, Tas F, Yilmaz M, Erdemci F, Sahin F, Ayaz H, Yilmaz EZ & Bolluk G, Placental vimentin expression in preeclampsia and gestational diabetes mellitus. *GORM*, 30 (2024) 10.